RESEARCH ARTICLE

Check for updates

High-silica zeolite Y: seed-assisted synthesis, characterization and catalytic properties†

Dali Zhu,[a,b] Linying Wang,*[a] Wenhao Cui,[a,b] Juan Tan,*[c] Peng Tian [ID] *[a] and Zhongmin Liu [ID] [a]

A facile solid seed assisted strategy has been developed for the synthesis of high silica zeolite Y. The crystal growth kinetics as a function of seed usage were studied, showing a positive relationship with the seed addition. A smaller seed size and higher seed SAR were found to be favorable for the crystallization of high silica zeolite Y. FTIR spectra revealed that the acidic hydroxyls in small SOD cages of high silica zeolite Y can transfer to supercages under the induction of pyridine, while this phenomenon is inconspicuous for conventional zeolite Y, which suggests the incremental utilization of the acid sites in the SOD cages following the increase of framework SAR. The high silica S-SY product possesses a larger amount of acid sites, higher acid strength and excellent (hydro)thermal stability, and thus exhibits higher catalytic cracking activity for model molecules and industrial heavy oil, which imply its promising future as a cracking catalyst for bulky hydrocarbons.

Introduction

Fluid catalytic cracking (FCC) is one of the largest catalytic processes in the world, which provides an effective route for converting heavy petroleum to gasoline, diesel and light gases.[1] The introduction of zeolite Y as the active component of FCC catalysts can be regarded as a milestone in the oil refinery industry, which revolutionized the FCC process and greatly increased the catalytic efficiency for fuel production.[2,3] Although a small amount of ZSM-5 additive was subsequently introduced into the catalyst to increase the gasoline octane number and the yields of light olefins,[4] zeolite Y remains to be the main active component of FCC catalysts. Nowadays, FCC catalysts account for more than 95% of the global zeolite catalyst consumption.[5]

Both fundamental research and industrial practices have demonstrated that a high framework SiO_2/Al_2O_3 ratio (SAR) of zeolite Y can help enhance the acid strength and (hydro) thermal stability,[6,7] which are essential for the prepared cracking catalyst to achieve high catalytic activity and stability.[8,9]

Unfortunately, as the direct synthesis of high silica zeolite Y has remained a challenging task over the past few decades, ultrastable Y (USY) prepared by complicated post-synthesis dealumination, such as steaming or acid leaching, becomes the unique choice for the preparation of FCC catalysts. However, the loss of crystallinity and mass, as well as the creation of defects and the dealumination gradient, is hard to avoid for the post-treatment process.[10–12] Relatively, direct synthesis of high silica Y is the most ideal route.

Considerable efforts have been devoted to the improvement of the framework SAR of zeolite Y since its successful application as an FCC catalyst. Hitherto, for the syntheses from an inorganic gel system, the highest SAR reported, however, is less than 6.5.[13] In theory, the use of organic structure directing agents (OSDAs) can reduce the number of framework Al atoms due to their lower charge density and thus facilitate the synthesis of high silica products, which have effectively worked for the syntheses of multiple zeolites.[14–16] Unfortunately, even with the help of OSDAs, the highest SAR of zeolite Y has long been limited to 9.0 (15-crown-5 as OSDA).[17] Moreover, significantly prolonged crystallization times are always observed when attempting to improve the SAR of zeolite Y, showing the high energy barriers of nucleation/crystallization of the high silica FAU framework. Recently, we developed a novel NOA-co strategy for the synthesis of zeolite Y,[18] which involves the use of FAU nucleus solution, bulky OSDAs and a low-alkalinity gel system. The combination of these three factors can address the synthesis bottlenecks in the nucleation and crystallization of high silica FAU frameworks, leading to a product with a SAR as high as 15.6 after a crystallization time of 6.5 days using

[a] National Engineering Laboratory for Methanol to Olefins, Dalian National Laboratory for Clean Energy, Dalian Institute of Chemical Physics, Chinese Academy of Sciences, Dalian 116023, China. E-mail: tianpeng@dicp.ac.cn, lywang@dicp.ac.cn
[b] University of Chinese Academy of Sciences, Beijing 100049, China
[c] Department of Catalysis Chemistry and Engineering, Faculty of Chemical, Environmental and Biological Science and Technology, Dalian University of Technology, Dalian, 116024, China. E-mail: tanjuan@dlut.edu.cn

This journal is © the Partner Organisations 2022

Inorg. Chem. Front., 2022, **9**, 2213–2220 | **2213**

tetrabutylammonium hydroxide (TBAOH) and tetraethylammonium hydroxide (TEAOH) as co-OSDAs. Very recently, during our manuscript preparation, Dusselier *et al.* reported the synthesis of high silica zeolite Y with a SAR up to 12.8 using 15-crown-5 and choline ions as co-OSDAs after a crystallization time of 5.0 days.[19]

In the present work, we explored the synthesis of high silica zeolite Y with the assistance of solid seeds using TBAOH as an OSDA. The impact of seed properties (such as addition amount, SAR and crystal size) on the synthesis was investigated and summarized. Well-crystallized high silica zeolite Y with a SAR up to 15.9 can be achieved in 2.0–3.5 days. Moreover, the acidity of the samples was systematically characterized. The cracking of model molecules and heavy oil was investigated to evaluate the catalytic cracking performance of the high silica products.

Experimental section

Materials and reagents

The chemical reagents used were sodium aluminate (50.7 wt% Al_2O_3, 41.9 wt% Na_2O, Shanghai Aladdin Industrial Co.), silica gel (99 wt%, Qingdao Meigao Reagent Co.), sodium hydroxide (NaOH, 99.9 wt%, Shanghai Aladdin Industrial Co.), tetrabutylammonium hydroxide (TBAOH, 40 wt% in H_2O, Shanghai Annaiji Chemical Reagent Co.), tetraethylammonium hydroxide (TEAOH, 35 wt% in H_2O, Shanghai Annaiji Chemical Reagent Co.), and tetraethyl orthosilicate (TEOS, 99 wt%, Tianjin Kemio Chemical Reagent Co.).

Commercial NaY zeolite with a SAR of 5.6 (named NaY_{ref}) was purchased from Shanghai Xinnian Petrochemical Additives Co. Ltd. USY with a SAR of 13.8 (product code: NKSN-28, in the NH_4^+ form) was purchased from Tianjin Shenneng Technology Co. Ltd, and it was prepared by a combination of hydrothermal dealumination and acid leaching.

Synthesis of nanosized zeolite seeds

A series of nanosized zeolite Y with different SARs were synthesized as seeds according to the NOA-co strategy reported by us recently. The samples were named Y_x, where x refers to the product SAR detected by XRF. The synthesis procedures of $Y_{10.2}$ and $Y_{14.1}$ were the same as those in our previous work. The synthesis of $Y_{6.3}$ has a little modification. In detail, FAU nucleus solution was first prepared from a clear solution with a molar composition of $1SiO_2 : 0.1Al_2O_3 : 0.01Na_2O : 1.2TEAOH : 18.3H_2O$. The above clear solution was heated at 50 °C for 12 h and then at 100 °C for 48 h. Then, 4.0 g silica gel was slowly added to a solution containing sodium aluminate (1.341 g), NaOH (0.554 g) and deionized water (28.656 g) to form an initial gel with a molar ratio of $1SiO_2 : 0.1Al_2O_3 : 0.24Na_2O : 24H_2O$. Subsequently, 4.89 g FAU nucleus solution was added dropwise into the above gel. The mixture was aged under agitation at room temperature for 2 h and then charged into a 50 mL stainless steel autoclave with a Teflon liner. The crystallization was con-

ducted in a static oven at 100 °C for 5.0 days. The product was centrifuged, washed with deionized water, and dried at 100 °C.

Milled seeds were prepared by the following procedure. Typically, 10 g of zeolite was dispersed in 50 g of deionized water and treated using milling apparatus for 2 hours. The slurry was then collected and dried to obtain the milled seed.

All the samples were calcined at 600 °C for 6 h before being used as seeds.

Seed-assisted synthesis of high silica zeolite Y (named S-SY)

In a typical run, 0.151 g of sodium aluminate was added to a solution containing 0.158 g of NaOH, 7.04 g of deionized water and 6.24 g of TBAOH. 1.8 g of silica gel was slowly added to the above solution under stirring to form a gel with a molar composition of $1SiO_2 : 1/40Al_2O_3 : 0.10Na_2O : 0.32TBAOH : 20H_2O$. Then, 0.18 g of calcined $Y_{14.1}$ seeds were added to the gel and aged under strong agitation at room temperature for 12 h. The final mixture was charged into a 50 mL stainless steel autoclave with a Teflon liner. The crystallization was conducted under rotation (45 rpm) at 120 °C for 2.5 days. The product was centrifuged, washed with deionized water, and dried at 100 °C. The sample was named $S-SY_{14.3}$, where 14.3 presents the product SAR detected by XRF.

For the preparation of H-form S-SY, the as-made sample was calcined in air at 600 °C for 6 h to remove the organic templates. Then, the calcined sample was ion exchanged with NH_4NO_3 solution (1.0 M) at 80 °C for 2 h (liquid/solid = 15) three times followed by calcination at 500 °C for 4 h in air.

Characterization

The crystalline phase and crystallinity of the as-made samples were determined using X-ray diffraction (XRD) patterns, which were collected on a PANalytical X'Pert PRO X-ray diffractometer with Cu Kα radiation (λ = 0.154059 nm, 40 kV and 40 mA). The inorganic elemental compositions of the samples were measured with a Philips Magix-601 X-ray fluorescence (XRF) spectrometer. The crystal size and morphology were observed using a scanning electron microscope (Hitachi SU8020). HRTEM images were obtained on a JEM-2100 transmission electron microscope. N_2 sorption–desorption experiments at 77 K were performed on a Micromeritics ASAP2020 volumetric adsorption analyzer. Before starting the measurement, the sample was degassed for 4 h under vacuum and at 350 °C.

Solid-state ^{29}Si MAS NMR spectra were recorded on a BrukerAvance III 600 spectrometer equipped with a 14.1 T wide-bore magnet using a 4 mmWVT double resonance MAS probe. The experiments were performed at a spinning rate of 8 kHz using high-power proton decoupling. The chemical shifts were referenced to Kaolinite at −91.5 ppm.

The hydrodynamic diameters of the milled seeds were determined by dynamic light scattering (DLS) analysis with a Malvern Zetasizer Nano. The seed slurry after milling treatment was dispersed using ultrasound in ethanol prior to measurement. Thermogravimetric analyses (TG-DSC) were carried out on a NETZSCH ATS 449 F3 analyzer from room temperature to 1250 °C (10 °C min^{-1}) under an air flow of

2214 | *Inorg. Chem. Front.*, 2022, **9**, 2213–2220

This journal is © the Partner Organisations 2022

20 mL min^{-1}. The acid properties of H-form zeolites were measured by NH$_3$-TPD on a Micromeritics 2920 chemical adsorption instrument. 200 mg of sample (40–60 mesh) was pretreated at 600 °C for 1 h under a flow of He. After pretreatment, the sample was cooled to 100 °C and saturated with NH$_3$ gas. Then, NH$_3$-TPD was performed under a flow of He (20 mL min^{-1}) from 100 to 600 °C (10 °C min^{-1}). The Brønsted and Lewis acidity of the Y zeolites was determined using the Fourier transform infrared spectra of pyridine adsorption/desorption (Py-FTIR). Spectra were recorded using a Bruker Tensor 27 instrument with a mercury cadmium telluride (MCT) detector. Typically, about 20 mg of zeolite powder was pressed into a self-supported wafer (diameter 13 mm). After activating in the IR cell at 450 °C for 30 min, the samples were cooled down to room temperature and saturated with pyridine. Then, a desorption experiment was performed at 150 °C, 250 °C, and 400 °C under vacuum. All the spectra are recorded at room temperature. The amounts of the Brønsted and Lewis acid sites were calculated by employing molar extinction coefficients from the literature.[20]

Catalytic test

Zeolite cracking activities with cumene and TIPB as probe molecules were determined in a fixed-bed quartz tubular reactor with an inner diameter of 8 mm at atmospheric pressure. For TIPB cracking experiment, 30 mg of the catalyst (40–60 mesh) diluted with 0.50 g quartz was packed in the reactor and activated in N$_2$ (40 mL min^{-1}) at 500 °C for 1 h prior to the reaction. TIPB was fed by passing the N$_2$ gas with the flow rate of 100 mL min^{-1} through a saturator containing TIPB at 70 °C, which gave a WHSV$_{TIPB}$ = 3.2 h^{-1}, and the reaction temperature varied from 130 to 170 °C. In the case of cumene cracking, 0.05 g of the catalyst (40–60 mesh) diluted with 0.10 g quartz was loaded into the reactor and activated in N$_2$ (40 mL min^{-1}) at 500 °C for 1 h prior to the reaction. The temperature of the catalyst bed varied from 180 to 210 °C in N$_2$. Subsequently, N$_2$ (40 mL min^{-1}) saturated with vaporized cumene at 40 °C was passed through the reactor, which gave a cumene WHSV of 3.7 h^{-1}. The effluents from the reactor were analyzed using an online Agilent 7890A GC equipped with a PONA capillary column and a FID detector.

For catalytic cracking of heavy oil, a fixed-bed stainless steel reactor with a catalyst loading of 4 g (20–40 mesh) was used. The diagram of the micro test system is given in Fig. S1.† The properties of the heavy oil used are given in Table S1.† The cracking reaction was operated at 482 °C with a reaction time of 75 s. The total amount of heavy oil used was 1.33 g. The gas products and liquid products were collected separately and analyzed by gas chromatography with FID detectors using a TDX-1 packed column and a PoraPLOT Q capillary column, respectively. The retention time of *n*-dodecane (216 °C) was taken as the boundary of gasoline and diesel. *n*-Dodecane was included into gasoline. The coke on the spent catalysts was measured by TG. For the preparation of a zeolitic catalyst, NH$_4^+$-form S-SY zeolite (35 wt%) was dispersed into a slurry of alumina sol (20 wt%) and clay (45 wt%). The mixture was dried at 120 °C for 12 h and calcined at 500 °C for 1 h. Prior to the cracking reaction, the catalysts were aged at 800 °C for 4 h or 17 h under 100% steam.

Results and discussion

The synthesis of high silica zeolite Y with the assistance of solid nanoseeds was explored based on a gel with a molar composition of 1SiO$_2$: 1/xAl$_2$O$_3$: 0.10Na$_2$O : 0.32TBAOH : 20H$_2$O. The detailed synthesis conditions and the corresponding XRD results are displayed in Table 1 and Fig. S2,† respectively. The properties of the seeds used are summarized in Fig. 1 and Table S2.† It can be seen that when x varies from 20 to 60, the XRD patterns of the products show typical FAU-type peaks, evidencing the formation of zeolite Y in high crystallinity. Further increasing the gel SAR to 70 results in the appearance of MEL impurity. The SAR of zeolite Y increases with that of the starting gel, and the highest SAR of 15.9 (sample S-SY$_{15.9}$) is achieved in the system with a gel SAR of 60. This value is even slightly higher than that obtained by the NOA-co strategy. In addition, the time for complete crystallization prolongs with the increase of gel SAR, implying the increased energy barriers for the growth of the high silica FAU framework. It is noted that for the synthesis of zeolite Y with a comparable SAR, the crystallization time herein is obviously shorter than that used in the NOA-co strategy (*e.g.*, 3.5 days *vs.* 6.5 days for zeolite Y with a SAR of 15–16).

Fig. 2a shows the SEM image of sample S-SY$_{15.9}$, which presents an aggregate morphology consisting of octahedral crys-

Table 1 Syntheses and product compositions of the high silica S-SY zeolites

Sample	x^a	Yield^b (%)	Time (day)	Product Phase	SAR^c	Unit cell composition^d
S-SY$_{11.8}$	20	56.7	2.0	Y	11.8	(H$_2$O)$_{38.2}$Na$_{17.5}$TBA$_{10.3}$(Si$_{164.2}$Al$_{27.8}$O$_{384}$)
S-SY$_{14.3}$	40	42.6	2.5	Y	14.3	(H$_2$O)$_{33.6}$Na$_{13.0}$TBA$_{10.6}$(Si$_{168.4}$Al$_{23.6}$O$_{384}$)
S-SY$_{15.9}$	60	34.2	3.5	Y	15.9	(H$_2$O)$_{20.0}$Na$_{10.7}$TBA$_{10.7}$(Si$_{170.6}$Al$_{21.4}$O$_{384}$)
S-SY$_{MEL}$	70	32.0	4.0	Y + MEL	—	—

^{a} Initial gel: 1SiO$_2$: 1/xAl$_2$O$_3$: 0.1Na$_2$O : 0.32TBAOH : 20H$_2$O (10 wt% addition of Y$_{14.1}$ seeds). The crystallization temperature is 120 °C. ^{b} Yield was calculated based on the dry mass of SiO$_2$ and Al$_2$O$_3$ ($M_{product}$/$M_{(gel+seeds)}$ × 100%). ^{c} Measured by XRF. ^{d} Calculated based on the results of TG-DSC analysis and XRF of the samples.
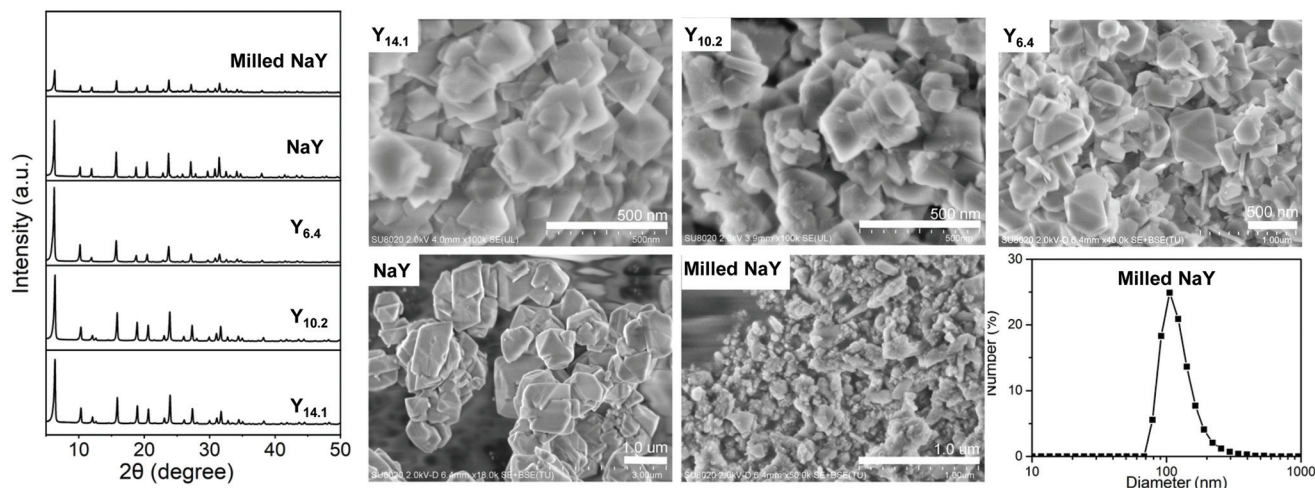
Fig. 1 XRD patterns (left) and SEM images (right) of the seeds employed for the synthesis of high silica zeolite Y; down-right: particle size distribution of the milled NaY.
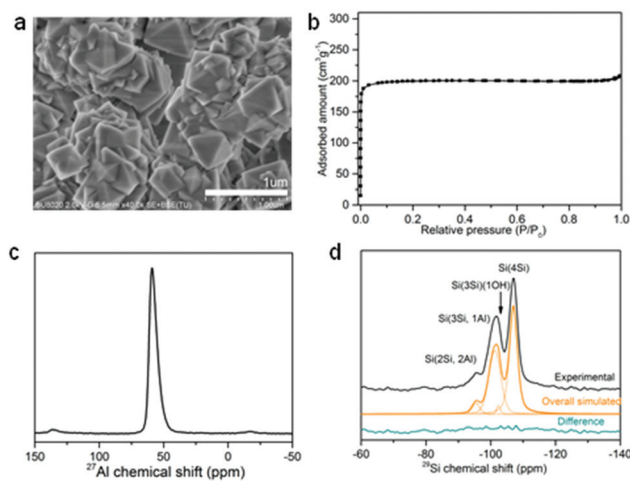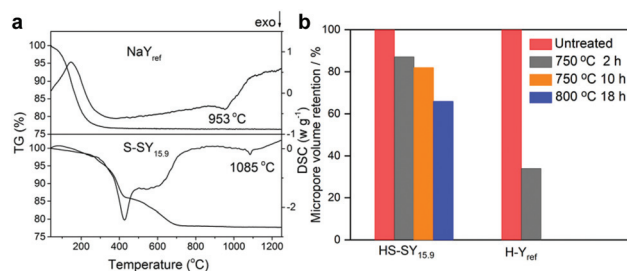

Fig. 2 (a) SEM image, (b) N_2 adsorption–desorption isotherms, (c) ^{27}Al and (d) ^{29}Si MAS NMR spectra of the sample S-SY$_{15.9}$. The as-made sample for a, c and d, and the calcined sample for b.

−107 and −100 ppm together with weak shoulders at −102 and −95 ppm are ascribed to Si(4Al), Si(3Si,1Al) and Si(3Si) (OH), Si(2Si,2Al) species, respectively. Based on the deconvoluted ^{29}Si NMR spectrum, the framework SAR of S-SY$_{15.9}$ is calculated to be 16.0, in good agreement with the result of XRF. In addition, the unit cell compositions of the samples are calculated and listed in Table 1. Clearly, from S-SY$_{11.8}$ to S-SY$_{15.9}$, the number of TBA$^+$ per unit cell shows a slight increase, while the number of Na$^+$ cations drops obviously.

The (hydro)thermal stability of zeolites, which is strongly related to the framework SAR, is a crucial factor for industrial applications. From Fig. 3a, the TG–DSC curves show that the structure of conventional NaY$_{ref}$ starts to collapse at 950 °C, while those of S-SY$_{15.9}$ remain stable until 1085 °C, evidencing the good thermal stability of the high silica product. The hydrothermal stability tests also give similar results (Fig. 3b). Herein, H-form samples were used to investigate the hydrothermal stability, because the existence of the sodium cation may hasten the structural deterioration under high-temperature steam conditions. It is clear that after 100% steam treat-
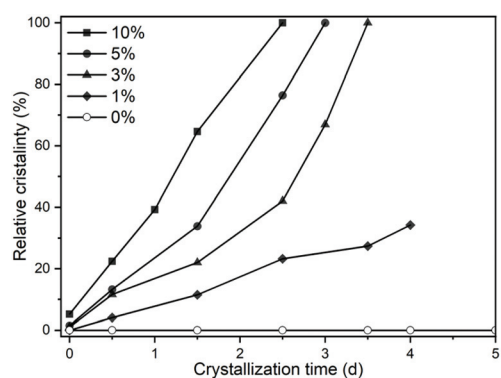
tals, and no amorphous material could be observed, suggesting the high purity of the sample. The textural properties of S-SY$_{15.9}$ were characterized using N_2 adsorption–desorption isotherms. As illustrated in Fig. 2b, the sample has a typical Langmuir-type curve. A steep adsorption increase occurs in the curve at a low relative pressure of $10^{-6} < P/P_0 < 0.01$, which is due to the filling of micropores by N_2. From Table S2,† the BET surface area and micropore volume of S-SY$_{15.9}$ are 634 m^2 g^{-1} and 0.29 cm^3 g^{-1} respectively, confirming its good crystallinity.

The local atomic environments of the as-made S-SY$_{15.9}$ were characterized by solid-state MAS NMR. The ^{27}Al MAS NMR spectrum (Fig. 2c) gives one sharp signal at 58.5 ppm associated with the framework tetrahedral-coordinated Al species. The ^{29}Si MAS NMR spectrum of S-SY$_{15.9}$ (Fig. 2d) presents four distinct sites for Si atoms. The strong resonances centered at

Fig. 3 Thermal stability and hydrothermal stability of the sample S-SY$_{15.9}$ compared to commercial Y (NaY$_{ref}$ and HY$_{ref}$). (a) TG-DSC curves and (b) loss of micropore volume after different hydrothermal treatments. The structural collapse temperatures of the samples are labeled in (a). The micropore volume of each fresh sample is defined as 100% in (b).

2216 | *Inorg. Chem. Front.*, 2022, **9**, 2213–2220

This journal is © the Partner Organisations 2022

ment at 750 °C or 800 °C, H-form S-SY$_{15.9}$ retains an obviously higher micropore volume than HY$_{ref}$. These results highlight the outstanding (hydro)thermal stability of S-SY$_{15.9}$, which should be attributed to its higher framework SAR.

To clarify the role of solid seeds, synthesis experiments without the addition of seeds and with various amounts of seeds were carried out. From Fig. 4, it can be found that the crystallization of zeolite S-SY was strongly dependent on the presence of seeds. Without seeds, only amorphous material can be obtained from the starting gel. In the presence of 1 wt% seeds, the crystallization can be initiated but in a much slow rate. Even after a crystallization time of 4.5 days, the product has extremely low crystallinity. On further increasing the seed amount, all syntheses can yield well-crystallized FAU-type material and the crystallization kinetics hasten with increasing seed addition. This evidences the important role of seeds in the synthesis of high silica zeolite Y. Compared with the NOA-co strategy, the synthesis with solid seeds involves rapid crystal growth without an induction period, giving rise to a shortened crystallization time. It is speculated that the amount of effective seeds in the FAU nucleus solution in the NOA-co strategy should be lower than that of solid nanoseeds, which causes its relatively slow crystallization kinetics.

Three solid nanoseeds, Y$_{6.4}$, Y$_{10.2}$ and Y$_{14.1}$ with a similar size but different SAR (Fig. 1 and Table S2†), were employed for synthesis to learn the effect of the seed SAR on crystallization. As presented in Table 2, with the addition of 3 wt% seeds, the induction activity of the seeds shows a positive relationship with their SAR. The product mainly consists of an amorphous material when using Y$_{6.4}$ as seeds. On increasing the seed SAR to 10.2, FAU becomes the main product phase together with a small amount of amorphous material. On further increasing the seed SAR to 14.1, well-crystallized zeolite Y can be readily achieved. With the addition of 10 wt% seeds, the difference in inducing activity among the seeds is hard to diminish, implying the excessive addition of seeds. Moreover, it is noted that the product SAR has an incremental trend with the increase of seed SAR, which demonstrates that

Table 2 Effect of the SAR of solid seeds on the synthesis

Sample[a]	Seeds (wt%)	Product	
		Phase	SAR[b]
1	3% Y$_{6.3}$	Amor + FAU	—
2	3% Y$_{10.2}$	FAU + amor	—
3	3% Y$_{14.1}$	FAU	14.1
4	10% Y$_{6.3}$	FAU	12.0
5	10% Y$_{10.2}$	FAU	13.1
6(S-SY$_{14.3}$)	10% Y$_{14.1}$	FAU	14.3

[a] The synthesis system is based on S-SY$_{14.3}$ in Table 1 except for the change of seeds. The crystallization times for the syntheses with 3% and 10% seed addition are 3.5 and 2.5 days, respectively. [b] Measured by XRF.

the seeds, at least part of them, are involved in the crystallization of high-silica zeolite Y.

Micrometer-sized commercial NaY (SAR = 5.6) and its milled product were further used as seeds to investigate the effect of the seed size on the synthesis. Fig. 1 shows the SEM images of NaY and milled NaY. It can be seen that the NaY crystals have a size of 1–2 μm, which are broken into irregular small particles after ball-milling treatment. The average particle size of milled NaY is about 100–200 nm. The synthesis results are displayed in Fig. 5. With the addition of NaY as seeds, the crystallization was not completed even after 5 days. The use of milled seeds, however, can effectively hasten the crystallization, leading to a well-crystallized high silica product after 2.5 days. Such a crystallization duration was similar to that of the above Y nanoseeds. These results indicate that the seeds with a small particle size are more effective in inducing the crystallization of high silica zeolite Y. The possible reason is that small crystals possess a larger external surface, which provides more surface for crystal growth.[21] Additionally, the synthesis with S-SY$_{14.3}$ as seeds was also carried out to learn

Fig. 4 Growth curves of high silica S-SY zeolite based on the gel system of S-SY$_{14.3}$ with different amounts of seeds.

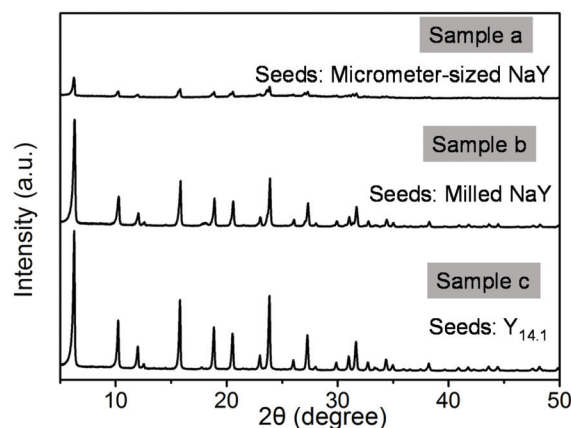**Fig. 5** XRD patterns of the solid products obtained from the synthesis system of S-SY$_{14.3}$ (Table 1) except with 10 wt% addition of NaY (a), milled NaY (b) and S-SY$_{14.3}$ (c) as seeds. Samples (b) and (c) were hydrothermally synthesized at 120 °C for 2.5 days, while for (a) the crystallization conditions were 120 °C for 5 days.

This journal is © the Partner Organisations 2022

Inorg. Chem. Front., 2022, **9**, 2213–2220 | **2217**

the possibility of the product itself as seeds (Fig. 5). Interestingly, zeolite Y with high crystallinity can be readily obtained after a crystallization of 2.5 days. Considering that S-SY$_{14.3}$ has a comparable crystal size to NaY, its effectiveness for the seeded growth of high silica zeolite Y confirms the stronger induction ability of high silica Y seeds.

The acid properties of the protonated S-SY zeolite were investigated by NH$_3$-TPD and FT-IR. For comparison, a conventional Y zeolite (HY$_{ref}$) was used as a reference sample. From the NH$_3$-TPD profiles (Fig. 6a), there are two desorption peaks at about 150–300 °C and 300–550 °C for both samples, which correspond to weak and strong acid sites, respectively. It is clear that high silica HS-SY$_{14.3}$ possesses a significantly larger amount of strong acid sites and higher acid strength than HY$_{ref}$. Fig. 6b presents the FTIR spectra of the hydroxyl groups

of the samples. The bands at 3630 cm^{-1} and 3550 cm^{-1} are associated with the acidic hydroxyls located in supercages and SOD cages respectively, while the band around 3742 cm^{-1} belongs to the isolated external silanols.[22,23] The FTIR spectra of the samples with pyridine desorption at different temperatures are shown in Fig. 6c and d. Both Brønsted and Lewis acid sites can be observed for the samples, evidencing the occurrence of the dealumination process. The relatively low proportion of Brønsted acid sites (B/(B + L)) on H–Y$_{ref}$ is consistent with its lower framework SAR and inferior (hydro)thermal stability. On increasing the desorption temperature from 250 °C to 400 °C, the intensity of Brønsted acid sites shows a decrease, especially for the HY$_{ref}$ sample. These results evidence a larger amount of Brønsted acid sites and stronger acidity of HS-SY$_{14.3}$. Moreover, from Fig. 6d, both the acidic hydroxyls in the supercages and SOD cages of HS-SY$_{14.3}$ show a clear decrease after pyridine adsorption at 150 °C. However, for conventional HY$_{ref}$, the acidic hydroxyls in the SOD cages remain less changed and mainly the acid sites located in the supercages are accessible. It implies that the Brønsted acid sites in the SOD cages of HS-SY$_{14.3}$ can transfer to supercages when the pyridine probe molecule is in close proximity,[24] but this proton transfer is difficult for conventional HY$_{ref}$. Summing up, acidity characterization using the NH$_3$-TPD and pyridine-adsorbed FTIR spectra demonstrates that HS-SY$_{14.3}$ possesses better acid site accessibility, higher acid strength and larger acid density.

1,3,5-Triisopropylbenzene (TIPB) cracking and cumene cracking were used as model reactions to assess the catalytic activity of HS-SY$_{14.3}$. A conventional H–Y zeolite was used as a reference catalyst. As the kinetic diameter of TIPB (0.95 nm) is larger than the pore opening of zeolite Y (0.73 nm), the cracking performance of TIPB is closely related to the acidity on the external surface of the samples. From Fig. 7a and b, HS-SY$_{14.3}$ exhibits both high activity and high selectivity to deep cracking products as compared to H–Y, implying the abundant strong acid sites on the external surface of HS-SY$_{14.3}$. Moreover, the cumene molecule has a relatively small diameter, and can
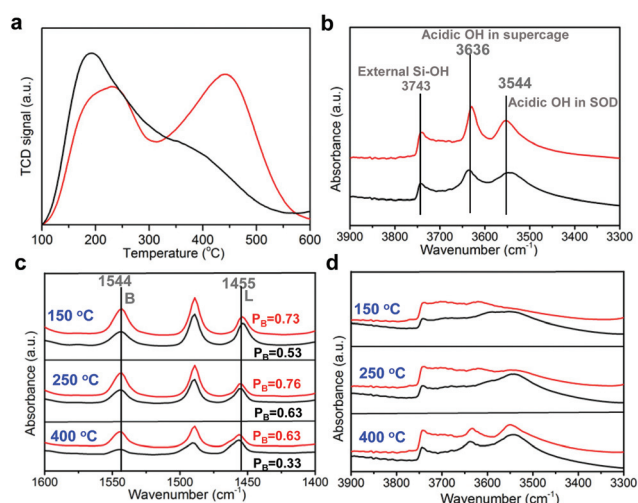
Fig. 6 The acid properties of the samples (HS-SY$_{14.3}$, red line; HY$_{ref}$, black line). (a) NH$_3$-TPD profiles, (b) FT-IR spectra of hydroxyl groups and (c and d) FT-IR spectra (pyridine and OH region) after pyridine desorption at different temperatures. PB shown in (c) stands for the proportion of Brønsted acid sites (B/(B + L)).
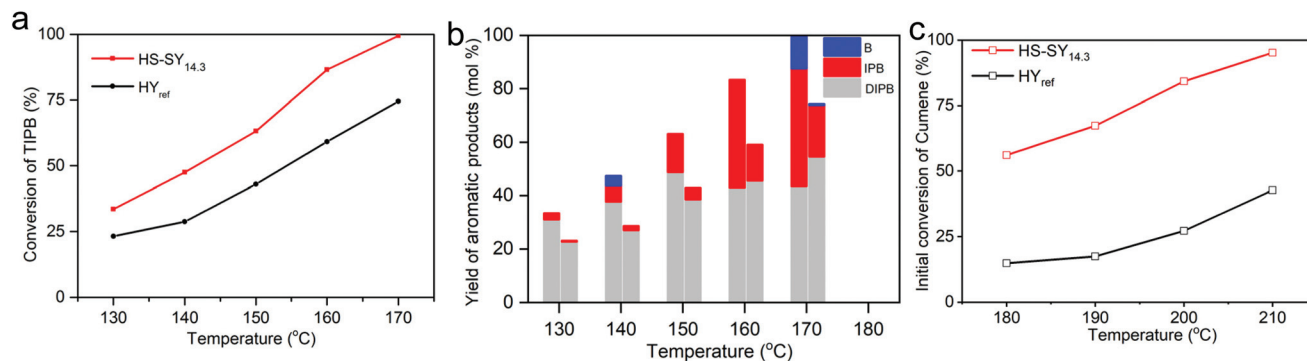
Fig. 7 The comparison of the catalytic cracking activity of HS-SY$_{14.3}$ and HY zeolites. (a) Initial activity of TIPB cracking at different reaction temperatures and (b) aromatic product yields of TIPB cracking (HS-SY$_{14.3}$, left; HY, right). WHSV$_{TIPB}$ = 3.2 h^{-1}. B, IPB and DIPB represent benzene, cumene and diisopropylbenzene, respectively. (c) Initial conversion of cumene *versus* reaction temperature, vaporized cumene (40 °C) in N$_2$ as the feed, flow rate = 40 mL min^{-1}, and WHSV$_{cumene}$ = 3.7 h^{-1}.

2218 | *Inorg. Chem. Front.*, 2022, **9**, 2213–2220

This journal is © the Partner Organisations 2022

Table 3 Heavy oil cracking results on the S-SY-based catalyst and USY-based catalyst

Items (wt%)	S-SY-based catalyst-4 h[a]	USY-based catalyst-4 h[a]
Dry gas	1.68	1.67
Liquid petroleum gas (LPG)	17.51	17.30
Gasoline	53.59	51.04
Diesel	11.26	12.08
Heavy oil	9.85	12.61
Coke	6.11	5.30
Conversion (excluding coke)	84.04	82.09
Conversion	90.15	87.37
Gasoline + diesel	64.85	63.12
LPG + gasoline + diesel	82.36	80.42
Diesel/gasoline ratio	0.21	0.24

[a] The catalysts were aged under 100% steam at 800 °C for 4 h before the catalyst test.

diffuse into the micropores of zeolite Y. The acid sites located in both the cages and external surface of zeolite Y can catalyze the cracking of cumene. From Fig. 7c, superior cumene conversion on HS-SY$_{14.3}$ can be observed than on H–Y$_{ref}$, which should be owing to the larger amount of strong acid sites and higher acid strength on HS-SY$_{14.3}$. These results demonstrate the excellent catalytic cracking activity of the HS-SY zeolite.

Heavy oil cracking was further carried out to evaluate the catalytic cracking performance of the high silica S-SY$_{14.3}$ zeolite for industrial feedstock. Herein, a catalyst containing 35 wt% zeolite, 20 wt% alumina and 45 wt% clay was prepared to simulate the component of industrial FCC catalysts.[25] For comparison, a commercial USY zeolite was used for the preparation of a reference catalyst. All catalysts were aged under 100% steam at 800 °C for 4 h before the catalyst test. Table 3 lists the results of heavy oil catalytic cracking. Compared with the USY-based reference catalyst, the S-SY-based catalyst shows a higher heavy oil conversion. Although the coke deposition on the S-SY-based catalyst is slightly higher than that on the USY-based catalyst, the gasoline yield and total yield of (LPG + gasoline + diesel) on the former are ~2.5 wt% and 2.0 wt% higher than those on the latter, respectively. Furthermore, the catalysts after treatment under 100% steam at 800 °C for 17 h were also evaluated for heavy oil cracking. The results are presented in Table S3.† Both catalysts show a decrease of heavy oil conversion, as compared with the corresponding 4 h-aged catalysts. However, the S-SY-based catalyst still has higher conversion than the USY-based catalyst. These results evidence the good catalytic cracking performance of the high silica S-SY zeolite for heavy oil conversion.

Conclusions

High silica zeolite Y with a framework SAR up to 15.9 has been synthesized using TBAOH as the OSDA with the assistance of solid seeds. Both the seed amount and seed properties are found to affect the crystallization of high silica zeolite Y. The

crystallization rate increases with the increase of seed amount in the investigated range of 0–10 wt%, and the seeds with a higher SAR and smaller crystal size are more effective for the synthesis. Moreover, the characterization results demonstrate that the high silica zeolite Y possesses excellent (hydro) thermal stability, a larger amount of Brønsted acid sites and stronger acidity than conventional zeolite Y. The acidic hydroxyls in small SOD cages of high silica zeolite Y can transfer to supercages under the induction of basic molecules and contribute to its larger acid amount determined by NH$_3$-TPD and pyridine-adsorbed FT-IR. As a result, the high silica material exhibits superior catalytic activity in the cracking reactions of hydrocarbons and industrial heavy oil.

Conflicts of interest

There are no conflicts to declare.

Acknowledgements

Notes and references

1 E. T. C. Vogt and B. M. Weckhuysen, Fluid catalytic cracking: recent developments on the grand old lady of zeolite catalysis, *Chem. Soc. Rev.*, 2015, **44**, 7342.

2 W. Vermeiren and J.-P. Gilson, Impact of Zeolites on the Petroleum and Petrochemical Industry, *Top. Catal.*, 2009, **52**, 1131.

3 J. Garcia-Martinez, K. Li and G. Krishnaiah, A mesostructured Y zeolite as a superior FCC catalyst - from lab to refinery, *Chem. Commun.*, 2012, **48**, 11841.

4 M. A. den Hollander, M. Wissink, M. Makkee and J. A. Moulijn, Gasoline conversion: reactivity towards cracking with equilibrated FCC and ZSM-5 catalysts, *Appl. Catal., A*, 2002, **223**, 85.

5 X. Meng, L. Wang and F.-S. Xiao, *Zeolites in Sustainable Chemistry*, Springer, Berlin Heidelberg, 2016, p. 271.

6 N. Wang, M. Zhang and Y. Yu, Distribution of aluminum and its influence on the acid strength of Y zeolite, *Microporous Mesoporous Mater.*, 2013, **169**, 47.

7 M. A. Kuehne, S. M. Babitz, H. H. Kung and J. T. Miller, Effect of framework Al content on HY acidity and cracking activity, *Appl. Catal., A*, 1998, **166**, 293.

8 F. Wang, L. Wang, J. Zhu, X. Zhang, Z. Yan, F. Fang, R. Tian, Z. Zhang and B. Shen, Effect of Si/Al ratio of the starting NaY on hydro-upgrading catalyst performance, *Catal. Today*, 2010, **158**, 409.

9 G. X. Niu, Y. Huang, X. Y. Chen, J. M. He, Y. Liu and A. He, Thermal and hydrothermal stability of siliceous Y zeolite

This journal is © the Partner Organisations 2022

Inorg. Chem. Front., 2022, **9**, 2213–2220 | **2219**

and its application to high-temperature catalytic combustion, *Appl. Catal., B*, 1999, **21**, 63.

10 F. Lonyi and J. H. Lunsford, The development of strong acidity in hexafluorosilicate-modified Y-type zeolites, *J. Catal.*, 1992, **136**, 566.

11 M. C. Silaghi, C. Chizallet and P. Raybaud, Challenges on molecular aspects of dealumination and desilication of zeolites, *Microporous Mesoporous Mater.*, 2014, **191**, 82.

12 R. A. Beyerlein, C. ChoiFeng, J. B. Hall, B. J. Huggins and G. J. Ray, Effect of steaming on the defect structure and acid catalysis of protonated zeolites, *Top. Catal.*, 1997, **4**, 27.

13 J. Y. Wang, P. S. Liu, M. Boronat, P. Ferri, Z. G. Xu, P. Liu, B. J. Shen, Z. D. Wang and J. H. Yu, Organic-Free Synthesis of Zeolite Y with High Si/Al Ratios: Combined Strategy of In Situ Hydroxyl Radical Assistance and Post-Synthesis Treatment, *Angew. Chem., Int. Ed.*, 2020, **59**, 17225.

14 M. B. Park, Y. Lee, A. Zheng, F. S. Xiao, C. P. Nicholas, G. J. Lewis and S. B. Hong, Formation pathway for LTA zeolite crystals synthesized via a charge density mismatch approach, *J. Am. Chem. Soc.*, 2013, **135**, 2248.

15 H. Sun, M. Wu, F. Han, W.-H. Wang, W. Wang, X. Luo and H. Chen, Crystallization of High Silica RHO Zeolite with Self-Assembled Cs+-18-crown-6 Sandwich Complex, *Cryst. Growth Des.*, 2019, **19**, 3389.

16 C. Martinez and A. Corma, Inorganic molecular sieves: Preparation, modification and industrial application in catalytic processes, *Coord. Chem. Rev.*, 2011, **255**, 1558.

17 C. Y. Li and L. V. C. Rees, The thermal-stability of Faujasites with different Si/Al ratios, *Zeolites*, 1986, **6**, 60.

18 D. L. Zhu, L. Y. Wang, D. Fan, N. N. Yan, S. J. Huang, S. T. Xu, P. Guo, M. Yang, J. M. Zhang, P. Tian and Z. M. Liu, A Bottom-Up Strategy for the Synthesis of Highly Siliceous Faujasite-Type Zeolite, *Adv. Mater.*, 2020, **32**, 2000272.

19 Q. Ke, I. Khalil, B. Smeyers, Z. Li, R. Oliveira-Silva, B. Sels, D. Sakellariou and M. Dusselier, A Cooperative OSDA Blueprint for Highly Siliceous Faujasite Zeolite Catalysts with Enhanced Acidity Accessibility, *Angew. Chem., Int. Ed.*, 2021, **60**, 24189.

20 C. A. Emeis, Determination of integrated molar extinction coefficients for infrared-absorption bands of pyridine adsorbed on solid acid catalysts, *J. Catal.*, 1993, **141**, 347.

21 J. Jiang, X. Wang, Y. Zhang, D. Liu and X. Gu, Fabrication of pure-phase CHA zeolite membranes with ball-milled seeds at low K+ concentration, *Microporous Mesoporous Mater.*, 2015, **215**, 98.

22 E. F. Rakiewicz, K. T. Mueller, T. P. Jarvie, K. J. Sutovich, T. G. Roberie and A. W. Peters, Solid-state NMR studies of silanol groups in mildly and highly dealuminated faujasites, *Microporous Mater.*, 1996, **7**, 81.

23 J. L. Agudelo, B. Mezari, E. J. M. Hensen, S. A. Giraldo and L. J. Hoyos, On the effect of EDTA treatment on the acidic properties of USY zeolite and its performance in vacuum gas oil hydrocracking, *Appl. Catal., A*, 2014, **488**, 219.

24 L. Lakiss, C. Kouvatas, J. P. Gilson, H. A. Aleksandrov, G. N. Vayssilov, N. Nesterenko, S. Mintova and V. Valtchev, Unlocking the Potential of Hidden Sites in Faujasite: New Insights in a Proton Transfer Mechanism, *Angew. Chem., Int. Ed.*, 2021, **60**, 26702–26709.

25 P. Liu, Z. Li, X. Y. Liu, W. Y. Song, B. W. Peng, X. Y. Zhang, S. F. Nie, P. H. Zeng, Z. D. Zhang, X. H. Gao and B. J. Shen, Steaming Drived Chemical Interactions of ZnClx with Y Zeolite Framework, Its Regulation to Dealumination/Silicon-Healing as well as Enhanced Availability of Brønsted Acidity, *ACS Catal.*, 2020, **10**, 9197.